aer

P.47

Functional Color Pages 1

ATMOSPHERIC AND ENVIRONMENTAL RESEARCH, INC.
CAMBRIDGE, MASSACHUSETTS

Extended Atmospheres of Comets and Outer Planet-Satellite Systems

IN-91-CR
78288

William H. Smyth
and
Max L. Marconi

Atmospheric and Environmental Research, Inc.
840 Memorial Drive
Cambridge, MA 02139-3794

March 30, 1992

Final Report

TECHNICAL REPORT STANDARD TITLE PAGE

1. Report No.	2. Government Accession No.	3. Recipient's Catalog No.

4. Title and Subtitle	5. Report Date
Extended Atmospheres of Comets and Outer Planet-Satellite Systems	March 1992
	6. Performing Organization Code

7. Author(s)	8. Performing Organization Report No.
William H. Smyth and Max L. Marconi	

9. Performing Organization Name and Address	10. Work Unit No.
Atmospheric and Environmental Research, Inc. 840 Memorial Drive Cambridge, MA 02139	11. Contract or Grant No. NASW-4329
	13. Type of Report and Period Covered Final Report 7/27/88 - 1/26/92
12. Sponsoring Agency Name and Address NASA Headquarters Headquarters Contract Division Washington, DC 20546	14. Sponsoring Agency Code
15. Supplementary Notes	

16. Abstract

For the hydrogen coma of comet P/Halley, both a Lyman-α image and extensive Lyman-α scan data obtained by the Pioneer Venus Orbiter Ultraviolet spectrometer as well as H-α ground-based spectral observations obtained by the University of Wisconsin Space Physics Group have been successfully interpreted and analyzed with our Monte Carlo particle trajectory model. The excellent fit of the model and the Halley data and the water production rate determined near perihelion (February 9, 1986) from December 13, 1985 to January 13, 1986 and from February 1 to March 7, 1986 are discussed here and are treated in more detail in one published paper and two additional papers in preparation. Studies for the circumplanetary distribution of atomic hydrogen in the Saturn and Neptune systems have been undertaken for escape of H atoms from Titan and Triton, respectively. The discovery of a new mechanism which can dramatically change the normal cylindrically symmetric distribution of hydrogen about the planet is discussed. The implications for the Titan-Saturn and Triton-Neptune are summarized and are discussed more fully in a paper currently in preparation.

17. Key Words (Selected by Author(s))	18. Distribution Statement
satellites, planets, comets	

19. Security Classif. (of this report)	20. Security Classif. (of this page)	21. No. of Pages	22. Price*
Unclassified	Unclassified	35	

*For sale by the Clearinghouse for Federal Scientific and Technical Information, Springfield, Virginia 22151.

TABLE OF CONTENTS

I. INTRODUCTION

The basic objective of this research has been to improve our understanding of the physical and chemical processes which produce the observed atomic comae of comets and extended hydrogen atmospheres of the outer planet-satellite systems. The strategy employed is divided into three steps: (1) acquire relevant observational data through collaborative efforts with others, (2) construct physically meaningful models for the extended atmospheres, and (3) analyze the relevant observational data with the models to extract physically meaningful information.

Much progress has been made in the third and final year of this project. All objectives of the three-year plan for modeling analysis of cometary atmospheres have been very successfully accomplished. These efforts have provided some fundamental advances in understanding the physics of the cometary H coma as well as some very interesting and useful results. One paper has already been published and two more are in preparation that describe various aspects of the H coma of Comet P/Halley. This research is summarized in Section II. For the research on the planet-satellite extended atmospheres, a new and very important mechanism for shaping its spatial morphology was discovered in the second project year and hence has dramatically altered the original three-year plan. The discovery provides a new basis for understanding the H distribution in the Saturn system produced by a Titan source in the light of new and recently reduced Voyager data (Shemansky and Hall, 1991). For the Neptune system, the new mechanism is operative, but an H torus produced by Triton would appear at present to be dominated by neutral-neutral collisions which will likely render the new mechanism ineffective. Research for the Saturn and Neptune systems is summarized in Section III and provides a new and exciting physical base for study and interpretation of these complex circumplanetary H distributions and their very important relationship to the planetary magnetospheres. A paper describing the new mechanism and its impact on the hydrogen torus of Titan and Triton is in preparation.

II. THE HYDROGEN COMA OF COMET P/HALLEY

1. Overview

The three-year plan for our research for the comae of comet P/Halley is summarized in Table 1. The first objective is to model the Pioneer Venus Orbiter ultraviolet spectro-

meter (PVOUVS) Lyman-α image of the comet acquired on February 2-6, 1986 by A. I. F. Stewart. This image, an initial and demanding two-dimensional test of the validity of our comet coma model, is only a small portion of the complete PVOUVS data set for comet P/Halley which involves a large number of radial scan profiles (i.e., one-dimensional data, not image data) that has been made available to AER through a collaborative effort with A. I. F. Stewart. The complete observational data set is summarized in Table 2 and includes, in addition to hydrogen observations, measurements for atomic oxygen and carbon as well as OH. Only the Lyman-α scan profiles for hydrogen were analyzed in this project. In addition, H-α emission data for the hydrogen coma of comet P/Halley obtained from ground-based observations by the University of Wisconsin Space Physics Group have also been successfully analyzed in the third project year in a collaborative effort undertaken with F. Scherb and F. L. Roesler. The two complementary data sets for the hydrogen coma were used to determine the water production rate of comet P/Halley near perihelion and thus filled a valuable gap in its overall heliocentric dependence of this production rate.

2. Analysis of the PVOUVS Lyman-α Image

The analysis of the PVOUVS Lyman-α image of the hydrogen coma of comet P/Halley was undertaken in the first project year, improved in the second project year and finally completed in the third project year and published (Smyth et al. 1991) in Science where a color version of the PVOUVS Lyman-α image was selected for the cover illustration. This paper, which is included in the appendix, shows that the fully time-dependent three-dimensional Monte Carlo particle trajectory model (MCPTM) of Combi and Smyth (1988 a,b) provides an accurate description of the complex physics of the coma and is able to very accurately model the PVOUVS Lyman-α image. This agreement is most gratifying in that it both verifies the underlying physics and documents the advantage and value of using a physically-based model.

3. Analysis of the PVOUVS Lyman-α Scan Profiles

The analysis of the Lyman-α scan profiles in Table 2 was initiated in the second project year and has been completed in the third project year. The MCPTM was used to fit the one-dimensional profiles and extract a water production rate on days indicated in Table

2. This research was presented at the 1991 fall AAS meeting of the Division for Planetary Sciences (Marconi and Smyth, 1991) and is currently being included in a paper in preparation (Smyth, Marconi, and Stewart 1992). These results are summarized below.

The output of the MCPTM is a two-dimensional brightness distribution of the solar Lyman α scattered by the coma hydrogen in the skyplane of the PVOUVS. The PVOUVS data for Lyman α from Halley's coma, however, consists of brightness profiles along narrow swaths of Halley's coma (see Stewart 1987 for a description of the data). As a result, the output from the model is convolved with the PVOUVS slit function and a model brightness profile along the swath is generated. The convolved model profile is then overlayed on the observed profile and shifted vertically until the profiles overlap in some optimal sense. In the overlaying process, the first few points around the peak are ignored due to multiple scattering of Lyman-α by an optically thick H column which is not currently fully treated in the MCPTM. An example of this procedure is illustrated in Figure 1. The average of the brightest data obtained on February 25, 1986 is compared to the model brightness along the swath calculated for that date. The generally excellent match is typical of the agreement between the data and model throughout the entire data set. The discrepancy between model and the data near the maximum of the profile is due to the multiple scattering of Lyman-α from the optically thick H column. The wings of the profile beyond about 10^7 km are somewhat limited in their ability to be compared due to large scatter in the data.

This procedure is repeated for selected observations between late December and early March. The many observations of the Lyman α are divided into sets (each set corresponding to one day of observations), and the data contaminated for example by light from other sources such as Venus or have the nucleus far from the center of the swath are discarded. From the remaining, the brightest data are selected since they cut closest to the nucleus and thus represent the best approximation to the instantaneous production rate. The data selected on a particular day are then averaged to improve statistics and compared to the model profile for that day. The results as summarized in Table 3 provide one production rate estimate per day for days when PVOUVS observed Halley's coma in Lyman-α.

Figure 2 is a comparison of the H_2O production rate vs day of the year given in Table 3 and those obtained by other observers. Perihelion is on day 40. The solid circles

represent a plot of the result of MCPTM modeling of the PVOUVS Lyman-α brightness measurements of Halley's hydrogen coma between late December 1985 to early March 1986. The other symbols represent H_2O production rates derived from other types of measurements for the period between early November 1985 to late April 1986. These do not exhaust all the measurements of comet Halley's production rates obtained in the relevant time interval, except possibly near perihelion. However, they are sufficient to illustrate how our results stand in reference to other determinations of H_2O production.

As is clear from Figure 2, toward late December 1985 and early January 1986, our production rates compare well with the production rates derived from IUE measurements of OH by Combi (1991) who also used the MCPTM approach and with those of Magee-Sauer et al. (1988) determination from $O(^1D)$ measurements. Beyond January 4 there is a gap in the PVOUVS data lasting to January 31. Continuous acquisition of high quality data resumed on about February 7. The MCPTM production rate rises from about 1.4×10^{30} s^{-1} to the peak of 1.9×10^{30} on February 10. The production rate remains high, varying about 1.5×10^{30} s^{-1}, until March 1 after which it falls with an apparent intent to join continuously with the IUE derived production rates of March 9 and beyond.

For the period between February 7 and March 7, there are a few H_2O production rate determinations from McCoy et al. (1991) rocket observation of Lyman α and Fink and Di Santi's (1990) O (^1D) observations. Within their estimated errors of about 50%, these determinations are quite consistent with the MCPTM results. Finally, there is also an extensive set of 18 cm OH radio observations for this time interval recently converted to H_2O production rates by Bockelée-Morvan et al. (1990). These are in poor agreement with the MCPTM results during this time. The interpretation of OH radio data, however, are complicated by a number of difficulties with the most insidious being the quenching of OH excited states. This is most severe at high production rates. Indeed Figure 2 shows that the agreement between MCPTM and the radio derived rates is only poor very near perihelion where the highest production rates occur.

Figure 3 compares our production rates with those determined by Stewart (1987) from the same data set. Although the two analyses lead to similar production rates at early times, there are notable differences after January 31, 1986. Our results are higher before and at perihelion. After perihelion both sets of derived rates oscillate with the oscillations in our rates appearing more pronounced. Finally, following March 1, 1986 our rates

display a rapid decrease while those of Stewart (1987) remains relatively flat. Both sets of rates are consistent with respect to other data except possibly in early March 1986 where Stewart's rates appear to be discontinuous relative to the other data starting after March 9. The differences in the production rates derived from the same data set are not surprising in view of the differences in the methods of conversion of brightness to production rates. For example, the solar Lyman α intensity used here is based on the most recent SME intensities, whereas the Stewart production rates were obtained using an older set of SME intensities. The differences between sets are between 10 and 20%.

4. Analysis of the Wisconsin H-α Observations

Observations for H-α emissions (6562.82 Å) from the coma of comet Halley were acquired in November and December of 1985 and in January, April and May of 1986 (Magee-Sauer 1988). Observations suitable for analysis were obtained in the preperihelion period (i.e. prior to February 9, 1986) and are summarized in Table 4 along with the observational and comet parameters. In Table 4, the H-α intensity values listed have been recently re-calibrated using H-α scans of a calibrated region of NGC 7000 (Scherb 1981). The NGC 7000 scans were taken at the same air masses as the comet scans when possible, and atmospheric transmission corrections were applied to scans taken at other air masses. Observations of alphaCMi (Breger 1976) were used to correct for variations of instrumental sensitivity at the different wavelengths used in the comet observations. AlphaCMi was also used to map the variation of sensitivity over the FOV at each wavelength. The projected area of the McMath telescope, which was designed for solar observations, was reduced at declinations north of zero degrees. The effective area was measured as a function of declination, and all observations were corrected for this characteristic.

All scans of the H-α line in Table 4 were taken with the center of the FOV 5' sunward of the comet head to avoid contamination from the (0,7,0) H_2O^+ emission line at 6562.8 Å (Lew 1976). Several scans were added together for each night in December 1985 to obtain an adequate signal to noise ratio. The scans were fitted with models based on Gaussian functions. Inputs to the fitting program were the scan data, the instrumental resolution profile, the number of Gaussians required to fit the spectral features, and initial estimates of the Gaussian parameters and the background level. The program varied the adjustable parameters until the Gaussians convolved with the instrumental profile produced

the best least-squares fit to the data. In the analysis of the H-α scans, the cometary H-α emission line profile was approximated by a single Gaussian. The non-Gaussian instrumental profile was approximated by a least-squares fit of two Gaussians to scans of laboratory spectral lamps or the terrestrial airglow [OI]6300 emission line. The H-α intensity values determined in this manner for the selected observations in December 1985 and January 1986 are summarized in Table 4.

The general approach to simulating the comet H coma is the Monte Carlo Particle Trajectory Model (MCPTM) which is described in detail by Combi and Smyth (1988 a,b). Whereas the modeling in the foregoing section was concerned with the computation of Lyman–α brightnesses (1215.67 Å), here it is the H-α brightness (6562.82 Å, air wave-length) of the coma which is of interest. The H-α brightness of an optically thin column is proportional to the product of the g-factor for the emission of the H-α radiation at 6562.82 Å and the column density. The g-factor in turn depends on the transition probabilities associated with all the levels of H which are able to contribute to the emission of H–α radiation and the corresponding intensities of the solar radiation which excite these H atom levels and lead to H-α emission by the process of de-excitation. The principal source of pumping the H atom to emit H-α photons is solar Lyman-β at 1025.72 Å. The H-α emission is not only due to the principal contribution from the 3p to 2s transition where the 3s state is populated from the 1s state by absorption of solar Lyman-β photons, but also because of several secondary contributions. These secondary contributions occur because of an additional contribution to the 3p state produced from the 2s state by absorption of solar H-α photons and because of additional H-α photons emitted in the 3p to 2s, 3s to 2p, and 3d to 2p transitions, where the 3p, 3s, and 3d states are populated by cascade from higher-level quantum states that are excited by the absorption of extreme ultraviolet solar radiation. The new g-factor at 1 AU including all of these transitions has recently been calculated by Shemansky (1991) and is given by the solid line in Figure 4 where the solar flux for the principal Lyman-β contribution is 3×10^9 photons cm^{-2} sec^{-1}, the same as used for the conventional g-factor given by the dashed-line calculation in Figure 4. The new g-factor is somewhat larger at 1 AU than the conventional g-factor and moreover has an additional local maximum due to a solar feature at 1025.77 Å consisting mainly of fine structure lines from the OI $3P\text{-}3D_O$ multiplet that has been included with the Lyman-β profile. This new velocity dependent g–factor is used in all modeling of the cometary H-α data in this paper.

The wavelength dependence of the g-factor discussed above is derived from data taken by OSO 8 during quiet sun conditions on August 19, 1976 and May 18, 1977 (Lemaire et al. 1978). We will assume following Donnelly and Pope (1973) that at 1 AU the total Lyman-β flux in the H Lemaire profile is 3.5 x 10^9 photons cm^{-2} s^{-1} while the corresponding Lyman-α profile is 3.1 x 10^{11} photons cm^{-2} s^{-1}. In order to compute the proper g-factor on another date, the Lyman-β flux is required on the days of observation which for the H-α data of interest here lie between early December 1985 and mid January 1986. The variation with solar cycle of the Lyman-β line shape is not known nor is the total flux. For the purposes of this investigation, it has been assumed that while the profile does not change in shape the total flux scales with the Lyman-α flux which is measured by SME and corrected for the comet location (Stewart 1991). Hence, if we designate the velocity dependent g-factor at a heliocentric distance of 1 AU and at the reference time t_o as g (v, t_o), the g-factor at time t is

$$g(v,t) = g(v, t_o)\frac{F(t)}{F(t_o)}\left(\frac{1}{R_h}\right)^2$$

where F (t) is the line-integrated Lyman alpha flux at time t and at 1 AU and R_h is the hydrogen atom heliocentric distance in AU units at time t. For H-α observations of interest here, F(t) is given in Table 5 and R_h is given in Table 4.

The MCPTM model was used to simulate H-α observations on those dates between December 5 and January 12 for which H-α measurements are listed in Table 4. When more than one H-α measurement was obtained per day, an average brightness value was used for model comparison. A sky plane H-α brightness distribution was generated by MCPTM for each of these days. The aperture response function was then applied on that part of the model sky plane brightnesses which corresponded to the location of the aperture. The new convolved sky plane brightness of the aperture was then converted to an integrated intensity of H-α emission over the aperture and compared to the measured value. Agreement of the model and measured H-α brightness values then determined the final H_2O production rates which are summarized in Table 5.

An example of the MCPTM model calculated image of the H-α brightness on the sky plane of the Earth is illustrated in Figure 5 for the January 4, 1986 observation. The

round circle corresponds to the location and size of the aperture on January 4. The brightness contours are quite circular about the location of Halley if one visually averages over the statistical variations. Over most of the field of view of the model calculation (i.e., 2×10^6 km by 2×10^6 km) the brightness of the H-α emission is of the order of 2 - 10 Rayleigh. The brightness in Figure 5 corresponds to an H_2O production rate of 6.3×10^{29}/s (see Table 5) and yields the same intensity in the aperture as measured after convolving the model brightness with the instrumental response function.

In Figure 6, the model-simulated H-α line profile (i.e., g-factor weighted velocity distribution along the line of sight) is shown for the brightness distribution as seen through the aperture in Figure 5 for the observation on January 4, 1986. The comet-earth velocity has not been included since it only corresponds to a shift in origin. Positive velocities reflect motion away from the earth. The distribution is nearly symmetrical about a velocity of zero as one might expect in the case of a nearly spherically symmetric coma and with the center of the aperture located here only 2.66×10^5 km from the comet nucleus. The line profile has a velocity dispersion of ~ 7 - 9 km/s which is about the velocity of most of H formed from the photodissociation of OH (~ 8 km/s). The convolution of the model line profile in Figure 6 with the spectral (10 km s^{-1} FWHM) instrumental profile (see the insert in Figure 7) is shown in Figure 7 to compare favorably with the observed line profile.

Figure 8 is a comparison between the H_2O production rates in Table 2 determined by the MCPTM analysis based on the H-α data and the H_2O production rates determined from other observations of Halley. The set of comparison rates is not exhaustive, but is sufficient to place rates derived here in perspective. The H-α data basically fills in the heliocentric dependence of the H_2O production rate from January 4 to January 13, 1986 when an outburst on the last day appears to have occurred. The only overlap of the H-α and Lyman-α data occurs on January 4, 1986 (i.e., day 4) where the H_2O production rate determined by the H-α data is 36% larger. This small difference may be caused by our inability to specify more accurately the relative g-factors for the H-α and Lyman-α emissions. The higher H-α emission may also be caused by its measurement being confined to a small region near the nucleus (see Figure 5) where it samples with more sensitivity the instantaneous increase in the H_2O production rate. In comparison, the Lyman-α emission samples a spatial region about the nucleus of several $\times 10^7$ km in width (see Figure 1) and hence captures a much longer time-averaged H_2O production rate that should be lower than the instantaneous production rate on January 4, 1986. The various

observations in Figure 8 are compared in more detail in the paper (Smyth, Marconi, Scherb and Roesler 1992) in preparation.

III. THE HYDROGEN DISTRIBUTION IN THE SATURN AND NEPTUNE SYSTEM

1. Overview

The spatial distribution of hydrogen in the circumplanetary environment of Saturn and Neptune are of particular interest in understanding the nature of the gas sources (i.e., satellites, planet, rings) and the way this material interacts with and determines the properties of the planetary magnetospheres. For the Saturn system, Voyager UVS measurements have provided H Lyman-α emission data, and a number of theoretical studies have been undertaken to understand the spatial distribution of neutral species and ion species. These are discussed below. For the Neptune system, there was no Voyager UVS detection of Lyman-α emission from H atoms in the magnetosphere, but studies for the Triton atmosphere (Strobel et al 1990; Summers and Strobel 1991) indicate that there should be a substantial global escape rate of H, H_2 and N from the satellite at energies suitable for formation of tori about the planet. Such gas tori should influence the plasma properties of the magnetosphere of Neptune (Zhang et al. 1991) and likely produce a collisionally thick torus of H (Cheng 1990) that emits Lyman-α radiation. This emission brightness, however, must be below the upper limit set by the Voyager UVS measurements (Broadfoot et al 1989; Shemansky 1990) which is hampered by the large LISM background.

Pre-Voyager three-dimensional models and analysis of available data for the H torus of Titan (Smyth 1981) showed that the hydrogen gas escaping from the satellite will form a torus completely surrounding Saturn with an enhancement in the density near the satellite. The initial interpretation of a limited amount of Voyager UVS Lyman-α data (Broadfoot et al. 1981; Sandel et al. 1982) supported this picture, suggesting a cylinder of hydrogen about the planet centered about the equatorial plan where the region inside 8 planetary radii was void of atomic hydrogen. Post-Voyager modeling (Ip 1985; Hilton 1987; Hilton and Hunten 1988) embraced this description in their simulations, and in the case of the latter two papers also considered a source of hydrogen from the planet as had been proposed earlier by Shemansky and Smith (1982). One-box, steady-state models studies (Eviatar and Podalak 1983; Richardson et al. 1986; Richardson and Eviatar 1987;

Eviatar and Richardson 1990) for gas tori and plasma tori to explore the overlap and consistency of the abundance of neutral and ion species have also been pursued, as have studies to explore the type of neutral tori generated by sputtering of neutrals from the inner satellites and rings (Johnson et al. 1989). The last two one-box model studies have been motivated by new information from a thorough and recent analysis of all Voyager UVS data for hydrogen in the Saturn system by Shemansky and Hall (1991) which indicates that the earlier picture of a cylindrical torus void of H atoms inside 8 planetary radii is incorrect.

The distribution of atomic hydrogen in the magnetosphere of Saturn is shown by Shemansky and Hall (1991) to be nonuniformly distributed in local time with (1) a preponderance of emission on the dusk side, (2) a density increasing radially inward to the top of the Saturn atmosphere, and (3) a density distribution having no cylindrically symmetric signature at Titan's orbit. This is in sharp contract to the initial analysis of a limited portion of the Voyager data noted above. A statistically significant peak in emission at 20 planetary radii in the antisolar region has been interpreted as strongly suggesting Titan as a partial source of atomic hydrogen in the system. This signature is, however, not what has been expected up to now upon theoretical grounds and suggest that a yet undiscovered mechanisms must be operative. The distinct asymmetry in the angular distribution of hydrogen about the planet with a maximum aligned approximately with the dusk terminator and a minimum in the predawn region again suggest an undiscovered mechanism other than sunlit hemisphere loss of hydrogen by the spinning planet which has been suggested by Shemansky and Hall (1991) as a possible mechanism for producing the asymmetric distribution. A new mechanism is discussed below.

2. A New Mechanism for the Saturn-Titan System

A nearly symmetric hydrogen torus about Saturn has been simulated in a variety of model studies as noted above. This symmetry was shown by Smyth (1981) to be produced naturally for H atoms that escape the gravitational field of Titan and then have insufficient energy to escape the 1/r gravitational potential of the planet, but have a lifetime sufficiently long so that they are able to make a number of angular orbits about the planet relative to the satellite location.

The addition of the accelerating force of solar radiation pressure will, however, eliminate this circumplanetary symmetry if the atom lifetime is sufficiently long. The effects of a constant perturbation force of solar radiation acceleration on a r^{-1} planetary gravitational potential have been studied using the planetary equations for the perturbed Keplerian motion problem and are well known. The geocorona problem for H atoms in near Earth orbit was first considered by Chamberlain (1979, 1980) in this manner (where the sun did not move in inertial space). This perturbation problem, including the constant angular motion of the Sun about the Earth, was then later shown to have an explicit analytic solution (Mignard and Hénon 1984; Deprit 1984). The basic time evolution of H-atom orbits about the planet are summarized by Chamberlain (1979) in three main effects: (1) high inclined orbits with eccentricities ≥ 0.4 are forced toward the ecliptic plane, (2) the perigees of direct orbits drift rapidly toward stable positions roughly westward (i.e. to the dusk side of the planet, (3) and orbits in or near such a stable point rapidly lower their perigees and end in collision with the atmosphere of the planet. This behavior can readily be verified by numerically integrating the equation of motion. Orbits with a larger semi-major axis will tend to collide with the planet earlier since the perturbation force of solar radiation acceleration pressure relative to gravity is greater at larger distances from the planet. This behavior will therefore selectively remove orbits at larger distance from the planet and will make the density on the dusk side of the planet larger than the dawn side, in agreement with the hydrogen distribution determined form the Voyager data by Shemansky and Hall (1991).

This evolutionary behavior for H atom orbits is, however, altered when the perturbation effects of the dominant J_2 non-spherical component of the gravitational field of Saturn (or Neptune) is considered. As is well known, the J_2 non-spherical component causes the line of perigees to precess about the planet and thereby limits the amount of time that radiation acceleration can act (at the otherwise stable positions westward of the planet for direct orbits) to lower the orbital eccentricity. The general result is that these two different precession periods interfere with each other and act so that the eccentricity oscillates in time and may or may not be sufficiently large to allow the hydrogen atom to collide with the planet, in the first or second approach to the otherwise favored westward position. This means that the H-atom collision rate for an ensemble of orbits generated by atoms escaping Titan (or Triton) will be time dependent. Atom collisions with the planet would then tend to occur primarily in waves separated by a time interval determined by the two separate precessing periods. The impact of this orbit evolution on the spatial

morphology of the hydrogen in the circumplanetary environment will therefore depend critically upon the relative value of the lifetime of the H atoms and the different H-atom planetary collision times.

The planetary equations for the perturbed Keplerian motion problem including both the solar radiation acceleration and the J_2 non-spherical gravity term were developed in the third project year and are summarized in Appendix B. These coupled equations have no known analytic solution and must be solved numerically. A numerical code to solve these equations for a set of initial conditions for the orbital elements has been developed and tested. The numerical solution has been used to investigage the relative importance of these H-atom planetary-colliding orbits in shaping the spatial morphology of hydrogen about Saturn. The essential results of the initial phase of this study are summarized below for the Titan-Saturn and Triton-Neptune systems and are discussed in more detail in the paper (Smyth and Marconi 1992) in preparation.

3. Implications for the Hydrogen Torus of Titan and Triton

Relevant time scales characterizing an ensemble of H atoms escaping from Titan or Triton and moving in bound orbits in the circumplanetary space of Saturn or Neptune are summarized in Table 6. For both Titan and Triton, the shortest time scale of a typical H atom is its Kepler orbital period about the planet with all other time scales being on average considerably larger. This insures the existence of a hydrogen distribution about the planet, but other time scales will influence the spatial character of this distribution. The relative values of these time scales, however, produce a situation for the hydrogen distribution in the Titan-Saturn system that is distinctly different than in the Triton-Neptune system as discussed below.

For the Titan-Saturn system, it should be noted that the H-atom lifetime, elastic H-H collision time, and radiative acceleration time have similar values even though (1) the H-atom lifetime in the planetary magnetosphere (Richardson and Sittler 1990) and solar wind environment and (2) the H-H atom elastic collision time in a very non-uniform gas distribution (Shemansky and Hall 1991) are both highly spatially variable. This means that H-H atom collisions are not in general important and that the residence time of H-atoms will be determined by the (1) H-atom magnetospheric/solar wind lifetime and (2) the

removal of H-atoms by collision with the planet which will be moderated by the interference of the J_2 precession which has a time scale ~ 3 times longer. Numerical computations verify this behavior and show that for a mean value of the solar Lyman-α flux, about 28% of the H atoms in the ensemble of orbits created by escape from Titan will collide with Saturn before they are removed from their orbits by charge-exchange and electron-impact loss processes. This means that radiation pressure and the J_2 gravitational term not only play a role in the residence time of H-atoms in the planetary environment but also greatly modify the spatial distribution of the atoms in space and should enhance the density of hydrogen on the dusk side of the dawn-dusk line due to the significant number of atoms that collide with the planet. Detailed model calculations which are to be proposed for future research work should verify this behavior and provide a quantative basis for study and interpretation of the new Voyager H Lyman-α data of Shemansky and Hall (1991).

For the Triton-Neptune system, the lifetime of H-atoms because of magnetospheric and solar wind loss processes is at least an order of magnitude larger than in the Saturn system and is furthermore significantly longer than all of the other Neptune time scales except perhaps the planet orbital period. Because of this fact, a larger steady state density of H-atoms can accumulate about Neptune, and the H-H elastic collision time becomes less than all time scales except the typical Kepler orbital period of the H atoms. A collisional torus will thus be formed, and the spatial distribution of the H-atoms about the planet will be significantly influenced by the steady-state velocity distribution that evolves. Since, however, there are still of order ten Kepler periods per collision on the average, the velocity distribution will not be determined by local conditions and local variables (i.e., density, average velocity and temperature), although they can be defined locally, cannot be locally related. Since the time scales for radiation acceleration and the J_2 gravitational term are significantly longer than the H-H collision time, the effects of these forces will not directly affect the orbital evolution of an individual atom orbit between collisions, but may perhaps have an overall effect on the envelope of these orbits in the circumplanetary space. The nature of the steady-state velocity distribution and the possible effects of the perturbation forces on the spatial envelope of the H-atom spatial distribution are new and exciting studies that are to be proposed for future research work.

IV. REFERENCES

Bockelée-Morvan D., Crovisier J., and Gérard E. (1990) Retrieving the Coma Gas Expansion Velocity in P/Halley, Wilson (1987 VII) and Several Other Comets from 18-cm OH Line Shapes, Astron. Astrophys. 238, 382-400.

Breger, M. (1976) Catalog of Spectrophotometric Scans of Stars, Astroph. J. Suppl. Series 32, 7-87.

Broadfoot, A. L. et al. (1981) Extreme Ultraviolet Observations from Voyager 1 Encounter with Saturn, Science 212, 206-211.

Broadfoot, A. L. et al. (1989) Ultraviolet Spectrometer Observations of Neptune and Triton, Science 246, 1459-1466.

Chamberlin, J.W. (1979) Depletion of Satellite Atoms in a Collisionless Exosphere by Radiation Pressure, Icarus 39, 286-294.

Chamberlin, J. W. (1980) Exospheric Perturbations by Radiation Pressure, Icarus 44, 651-656.

Cheng, A. F. (1990) Triton Torus and Neptune Aurora, Geophys. Res. Lett. 17, 1669-1672.

Combi, M.R. (1991) Private communication.

Combi, M.R., and Smyth, W. H. (1988a) Monte Carlo Particle Trajectory Models for Neutral Cometary Gases. I. Models and Equations, Ap. J. 327, 1026-1043.

Combi, M.R., and Smyth, W. H. (1988b) Monte Carlo Particle Trajectory Models for Neutral Cometary Gases. II. The Spatial Morphology of the Lyman-α Coma, Ap. J. 327, 1044-1059.

Deprit, A. (1984) Dynamics of Orbiting Dust Under Radiation Pressure, The Big Bang and George Lemaitre, Ed. A. Berger; D. Reidel Publishing Co., 151-180.

Donnelly, R. F., and Pope, J. H. (1973) The 1-3000 Å Solar Flux for a Moderate Level of Solar Activity for Use in Modeling the Ionosphere and Upper Atmosphere, NOAA Tech. Rep. ERL 276-SEL 25, U. S. Government Printing Office, Washington, D.C.

Eviatar, A. and Podolak, M. (1983) Titan's Gas and Plasma Torus, J. Geophys. Res. 88, 833-840.

Eviatar, A. and Richardson, J. D. (1990) Water Group Plasma in the Magnetosphere of Saturn, Annales Geophysicae 8, 725-732.

Fink U. and DiSanti A. (1990) The Production Rate and Spatial Distribution of H_2O For Comet P/Halley, Ap. J. 364, 687-698.

Hilton, D. A. (1987) A Partial Collisional Model of the Titan Hydrogen Torus, Ph. D. Thesis, Univ. of Arizona.

Hilton, D. A. and Hunten, D. M. (1988) A Partially Collisional Model of the Titan Hydrogen Torus, Icarus 73, 248-268.

Ip, W.-H. (1985) Titan's Hydrogen Torus, "The Atmosphere of Saturn and Titan" Workshop, Alpbach, Austria, 16 - 19 September, 1985, ESA SP-241.

Johnson, R. E., Pospieszalska, M. K., Sittler, E.C., Cheng, A. F., Lanzerotti, L. J. and Sieveka, E. M. (1989) The Neutral Cloud and Heavy Ion Inner Torus at Saturn, Icarus 77, 311-329.

Lemaire, P., Charra, J., Jouchoux, A., Vidal-Madjar, A., Artzner, G.E., Vial, J.C., Bonnet, R.M., and Skumanich, A. (1978) Calibrated Full Dish Solar H I Lyman-α and Lyman-β Profiles, Ap.J.Lett. 223, L55-L58.

Lew, H. (1976) Electronic Spectrum of H_2O^+, Can. J. Phys. 54, 2028-2049.

McCoy R.P., Meier R.R., Keller H.V., Opal C.B., Carruthers G.R. (1991) The Hydrogen Coma of Comet P/Halley Observed in Lyman α using Sounding Rockets, submitted to Astronomy and Astrophys.

Magee-Sauer, K.P. (1988) Ground-Based Fabry-Perot Observations of Neutral and Ionic Atoms and Molecules of Comet Halley, Ph.D. Thesis, Physics Dept.,.Univ. of Wisconsin, Madison.

Magee-Sauer, K., Roesler, F.L., Scherb, F. and Harlander, J. (1988) Spatial Distribution of O (^{1}D) from Comet Halley, Icarus 76, 89-99.

Magee-Sauer, K., Scherb, F., Roesler, F. L. and Harlander, J. (1990) Comet Halley O(^{1}D) and H_2O Production Rates, Icarus 84, 154-165.

Marconi, M. L. and Smyth, W. H. (1991) The Production of H_20 by Halley Close to Perihelion, Bull. AAS 23, 1168.

Mignard, F. and Hénon, M. (1984) About an Unsuspected Integrable Problem, Celestrial Mechanics 33, 239-250.

Richardson, J. D., Eviatar, A. and Siscoe, G. L. (1986) Satellite Tori at Saturn, J. Geophys. Res. 91, 8749-8755.

Richardson, J. D. and Eviatar, A. (1987) Limits on the Extent of Saturn's Hydrogen Cloud, Geophys. Res. Lett. 14, 999-1002.

Richardson, J. D. and Sittler, E. C. (1990) A Plasma Density Model for Saturn Based on Voyager Observations, J. Geophys. Res. 95, 12019-12031.

Roy, A. E. (1965) The Foundations of Astrodynamics, Macmillian Co., N. Y.

Sandel, B. R., et al . (1982) Extreme Ultraviolet Observations from Voyager 2 Encounter with Saturn, Science 215, 548-553.

Scherb, F. (1981) Hydrogen Production Rates from Ground-based Fabry-Perot Observations of Comet Kohoutek, Astrophys. J. 243, 644-650.

Shemansky (1990) Private communication.

Shemanksy, D.E. (1991) Private communication.

Shemansky, D. E. and Smith, G. R. (1982) Whence Comes the "Titan Hydrogen Torus", EOS Trans. AGU 63, 1019.

Shemansky, D. E. and Hall, D. T. (1991) The Distribution of Atomic Hydrogen in the Magnetosphere of Saturn, preprint.

Smyth, W. H. (1981) Titan's Hydrogen Torus, Ap. J. 246, 344-353.

Smyth, W. H. and Marconi, M. L. (1992) The Nature of the Hydrogen Torus of Titan and Triton, paper in preparation.

Smyth, W. H., Combi, M. R. and Stewart, A. I. F. (1991) Analysis of the Pioneer-Venus Lyman-α Image of the Hydrogen Coma of Comet P/Halley, Science 253, 1008-1010.

Smyth, W. H., Marconi, M. L., and Stewart, A. I. F. (1992) Analysis of Hydrogen Lyman-α Observations of the Coma of Comet P/Halley Near Perihelion, paper in preparation.

Smyth, W. H., Marconi, M. L., Scherb, F. and Roesler, F. L. (1992) Analysis of Hydrogen H-α Observations of the Coma of Comet P/Halley, paper in preparation.

Stewart, A. I. F. (1987) Pioneer Venus Measurements of H, O, and C Production in Comet P/Halley Near Perihelion, Astron. Astrophys. 187, 369-374.

Stewart, A. I. F. (1991) Private communication.

Strobel, D. F., Summers, M. E., Herbert, F. and Sandel, B. R. (1990) The Photochemistry of Methane in the Atmosphere of Triton, Geophys. Res. Lett. 17, 1729-1732.

Summers, M. E. and Strobel, D. F. (1991) Triton's Atmosphere: A Source of N and H for Neptune's Magnetosphere, Geophys. Res. Lett. 12, 2309.

Weaver H.A., Mumma M. J., and Larson H.P. (1987) Infrared Investigation of Water in Comet P/Halley, Astron. Astrophys. 187, 411-418.

Zhang, M., Richardson, J. D. and Sittler, E.C. (1991) Voyager 2 Electron Observations in the Magnetosphere of Neptune, J. Geophys. Res. 96, 19085-19100.

Table 1

COMETARY ATMOSPHERES: THREE-YEAR PLAN FOR MODELING ANALYSIS

P/Halley	First Year	Second Year	Third Year
H Coma	PVOUVS Lyman-α Image Data	• PVOUVS Lyman-α data scan • Wisconsin Hα line profile data	
O,C,OH, Comae			• PVOUVS O,C,OH scan data • Wisconsin O(6300Å) line profile data

Table 2

COMET P/HALLEY OBSERVATIONS FROM THE PIONEER VENUS ORBITER

	Date of Observation	Total Daily Observing Time (hr)	Observing Time per Species (hr)				
			H	O	C	OH	OTHER
1985	28 December	15	8	7	-	-	-
	29 December	15	7	8	-	-	-
	30 December	16	6	1	9	-	-
	31 December	16	5	3	-	8	-
1986	1 January	13	9	-	4	-	-
	2 January	20	4	15	1	-	-
	3 January	16	4	4	8	-	-
	4 January	15	4	3	-	8	-
	5 January	14	4	10	-	-	-
	6 January	14	7	-	7	-	-
	7 January	7	3	4	-	-	-
	30 January	3	3	-	-	-	-
	31 January	16	10	2	2	2	-
	1 February	11	5	2	2	2	-
	2 February*	18	18	-	-	-	-
	3 February*	19	19	-	-	-	-
	4 February*	19	13	1	2	1	2
	5 February*	19	17	-	-	-	2
	6 February*	19	17	-	-	-	2
	7 February	15	9	1	1	1	3
	8 February	11	7	2	2	-	-
	9 February†	16	8	2	2	2	2
	10 February	11	8	1	2	-	-
	11 February	16	9	1	2	1	3
	12 February	16	9	1	6	-	-
	13 February	19	12	6	1	-	-
	14 February	15	10	5	-	-	-
	15 February*	20	20	-	-	-	-
	16 February	16	10	4	2	-	-
	17 February	16	9	3	2	2	-
	18 February	18	11	2	2	3	-
	19 February	12	9	1	2	-	-
	20 February	19	12	2	2	2	1
	21 February	20	13	2	2	2	1
	22 February	16	13	1	1	1	-
	23 February	19	13	2	2	2	-
	24 February	19	13	2	2	2	-
	25 February	21	14	3	2	2	-
	26 February	14	6	3	3	2	-
	27 February	19	11	2	3	3	-
	28 February	22	14	3	2	3	-
	1 March	18	12	2	2	2	-
	2 March	19	11	3	2	3	-
	3 March	21	13	2	3	3	-
	4 March	21	13	3	2	3	-
	5 March	15	8	2	2	3	-
	6 March	20	12	3	2	3	-
	7 March	2	-	1	1	-	-

*Image data acquired on these days for hydrogen

†Perihelion

Table 3

H_2O Production Rate for Comet Halley Determined from the Lyman-α Observations

Date			Heliocentric Distance (AU)	H_2O Production Rate (10^{29} molecules s^{-1})
1985	Dec.	28	1.06	2.83
		29	1.59	2.91
		30	1.56	3.67
		31	1.53	3.34
1986	Jan.	1	1.49	3.25
		2	1.46	4.13
		3	1.43	4.30
		4	1.39	4.62
		5	1.36	4.64
		6	1.32	4.45
	Feb.	1	1.10	11.00
		3	.80	7.90
		4	.59	14.20
		8	.59	14.30
		9	.59	17.10
		10	.59	17.20
		11	.59	16.80
		12	.59	15.10
		13	.59	17.20
		14	.60	18.80
		15	.60	17.10
		16	.61	16.60
		17	.61	15.30
		18	.62	12.70
		19	.63	13.30
		20	.63	14.40
		21	.64	12.60
		22	.65	14.80
		23	.66	13.60
		24	.67	13.60
		25	.68	14.60
		26	.69	14.80
		27	.70	15.00
		28	.71	16.40
	March	1	.73	14.50
		2	.74	13.50
		3	.75	12.70
		4	.76	11.00
		5	.78	9.40
		6	.79	9.36
		7	.81	8.70

Table 4

Selected H-α Observations

Date	Start Time (UT)	Total Scan Time (minutes)	z† (deg)	R_h† (AU)	Δ† (AU)	H-α Intensity (Rayleighs)	Notes††
13 Dec 85	0546	13.8	65	1.295	0.793	1.6 ± 0.2	2 scans added
14 Dec 85	0324	35.1	40	1.279	0.803	1.5 ± 0.2	5 scans added
15 Dec 85	0353	30.3	46	1.267	0.823	1.2 ± 0.15	5 scans added
16 Dec 85	0456	12.1	62	1.248	0.844	1.1 ± 0.14	2 scans added
4 Jan 86	0212	7.7	60	0.959	1.222	4.1 ± 0.5	single scan
	0222	7.7	62	0.959	1.222	4.2 ± 0.5	" "
7 Jan 86	0204	7.6	62	0.918	1.272	5.7 ± 0.7	" "
	0213	7.5	64	0.918	1.272	5.2 ± 0.7	" "
	0222	7.5	66	0.918	1.272	5.2 ± 0.7	" "
8 Jan 86	0223	7.5	66	0.898	1.294	7.6 ± 1.0	" "
9 Jan 86	0155	11.9	63	0.888	1.311	7.9 ± 1.0	" "
12 Jan 86	0109	10.0	58	0.839	1.361	6.4 ± 0.8	" "
	0221	8.3	72	0.839	1.362	5.1 ± 0.6	" "
13 Jan 86	0212	7.3	72	0.828	1.372	13.7 ± 1.5	" "
	0222	5.6	74	0.828	1.372	12.5 ± 1.5	" "

† z is the zenith angle, R_h is the heliocentric distance of Comet Halley, Δ is the geocentric distance of Comet Halley.

†† For data where multiple scans are used, time and zenith angle given are average values.

Table 5

H_2O Production Rate for Comet P/Halley Determined from the H-α Observations

Date of Observation	Lyman-α Flux† at 1 AU (10^{11} ph/cm^2/s)	H_2O Production Rate (10^{29} s^{-1})
1985 Dec. 13	2.68	4.3 ± .5
14	2.66	4.1 ± .5
15	2.65	3.2 ± .4
16	2.62	2.8 ± .3
1986 Jan. 4	2.66	6.3 ± .8
7	2.64	8.3 ± .9
8	2.58	11 ± 1.4
9	2.55	11.6 ± 1.5
12	2.48	7.8 ± .9
13	2.46	17.5 ± 2

† Absolute error ± 15%; relative error 1 to 1.5% per year ± 5% (Rottman, 1992)

Table 6

COMPARISON OF TIME SCALES FOR CIRCUMPLANETARY H ATOM ORBITS

Satellite Source	Typical H-Atom Orbital Period[1] (s)	H-Atom Lifetime (s)	Elastic H-H Collision Time[2] (s)	Radiation Acceleration Time Scale[3] (s)	J_2 Gravitation Time Scale (s)	Planet Orbital Period (s)
Titan	1.38×10^6	$0.02 - 1 \times 10^8$	$\sim 0.2 - 1 \times 10^8$	$\sim 0.9 \times 10^8$	$\sim 2.7 \times 10^8$	9.30×10^8
Triton	5.10×10^5	$\geq 1 \times 10^9$	$\sim 0.3 - 1 \times 10^7$	$\sim 7 \times 10^8$	$\sim 3.4 \times 10^8$	5.20×10^9

1 Satellite orbital period is assumed.

2 For Saturn and Neptune, respectively, assumed an average H density of 10-50 cm^{-3} and 150-500 cm^{-3} and an average collision speed of 3.0 km s^{-1} and 2.2 km s^{-1}; a collision cross section of 3×10^{-15} cm^{-2} was adopted.

3 A mean solar integrated Lyman-α flux of 3.5×10^{11} photons/cm^2/s was assumed.

FIGURE CAPTIONS

Figure 1 Comparison of the Lyman-α Intensity Distribution Along the Scan for February 25, 1986. The brightness is in kilorayleighs, and the distance along the scan is in 10^6 km. The data is represented by the + symbol and the model fit is given by the solid line.

Figure 2 H_2O Production Rates for Comet Halley. The production rates in units of 10^{29} molecules/s is shown as a function of the day of the year from November 1985 to May 1986 for a variety of measurements. The symbols refer to the following:

Δ IUE
Combi (1991)

□ Magee-Sauer K., Scherb K., Roesler F.L., and Harlander J. Comet Halley and H_2O Production Rates, Icarus 84, 154-165 (1990).

x Bockelée-Morvan D., Crovisier J., and Gérard E. Retrieving the coma gas expansion velocity in P/Halley, Wilson (1987 VII) and several other comets from 18-cm OH line shapes. Astron. Astrophys. 238, 382-400 (1990).

\+ Weaver H.A., Mumma M. J., and Larson H.P. Infrared Investigation of water in comet P/Halley Astron. Astrophys. 187, 411-418 (1987).

◊ McCoy R.P., Meier R.R., Keller H.V., Opal C.B., Carruthers G.R., The Hydrogen Coma of Comet P/Halley Observed in Lyman α using Sounding Rockets, submitted to Astronomy and Astrophys. 1991.

* Fink U. and DiSanti A. The Production Rate and Spatial Distribution of H_2O For Comet P/Halley Ap. J. 364:687-698 (1990).

• MCPTM

Figure 3 H_2O Production Rate for Comet Halley. The solid dots represent the MCPTM Lyman-α results in Table 3, and the open dots are the earlier values of Stewart (1987).

Figure 4 G-factor for H-α Emission by Hydrogen Atoms Excited by Solar Radiation. The g-factor is shown as a function of heliocentric radial velocity of the H atom where negative velocity reflects motion towards the sun. The dotted line is the conventionally employed g-factor whereas the solid line is the g-factor which takes into account the contribution of a number of different solar excited states of H (see text for discussion).

Figure 5 Model Calculated Brightness of the H-α Emission for Comet P/Halley. H-α brightness contours in Rayleighs as generated by the MCPTM on the sky plane are shown for the observation of January 4, 1986. The circle indicates the location and size of the observing aperture on the sky plane. An H_2O production rate of 6.3 x 10^{29} molecules s^{-1} is required to match the measured brightness in the aperture. The sun is to the left.

Figure 6 Model Calculated H-α Line Profile. The model line profile for the observation of January 4, 1986 as seen from the Earth through the aperture illustrated in Figure 5 is shown as a function of Doppler velocity. The relative motion between the Earth and comet is not included. Positive velocities represent motion away from the Earth.

Figure 7 Comparison of Observed and Calculated H-α Line Profile. The observed line profile for January 4, 1986 is given by the solid line. The observed cometary H-α emission is the smaller feature centered at zero velocity. The larger feature centered at about -32 km s^{-1} is the H-α geocorona emission. The instrumental profile is given in the insert as a function of velocity and has a full width at half maximum of about 10 km s^{-1}. The corresponding model line profile (i.e., the profile in Figure 6 convolved with the instrumental profile) is given by the dashed line. A uniform background of 0.15 Rayleighs/(km/s) has been added to the convolved model profile to adjust it to the background level of the observation.

Figure 8 Comparison of Various H_2O Production Rates for Comet P/Halley. The H_2O production rates determined from the H-α observations are given in units of 10^{29} molecules s^{-1} and are compared as a function of the day of the year (i.e.,

0=Jan 1, 1986) with rates determined from various other Halley observations identified below. The day of perihelion is shown by the dotted line.

□ H_2O production rates determined from data for 6300 emission from atomic oxygen by Magee-Sauer et al. (1990).

* H_2O production rates determined from data for Lyman-α emission from atomic hydrogen by Smyth, Marconi and Stewart (1992).

Δ H_2O production rates determined from IUE data for OH emission by Combi (1991).

• H_2O production rates determined from MCPTM analysis of H-α observations (Table 5).

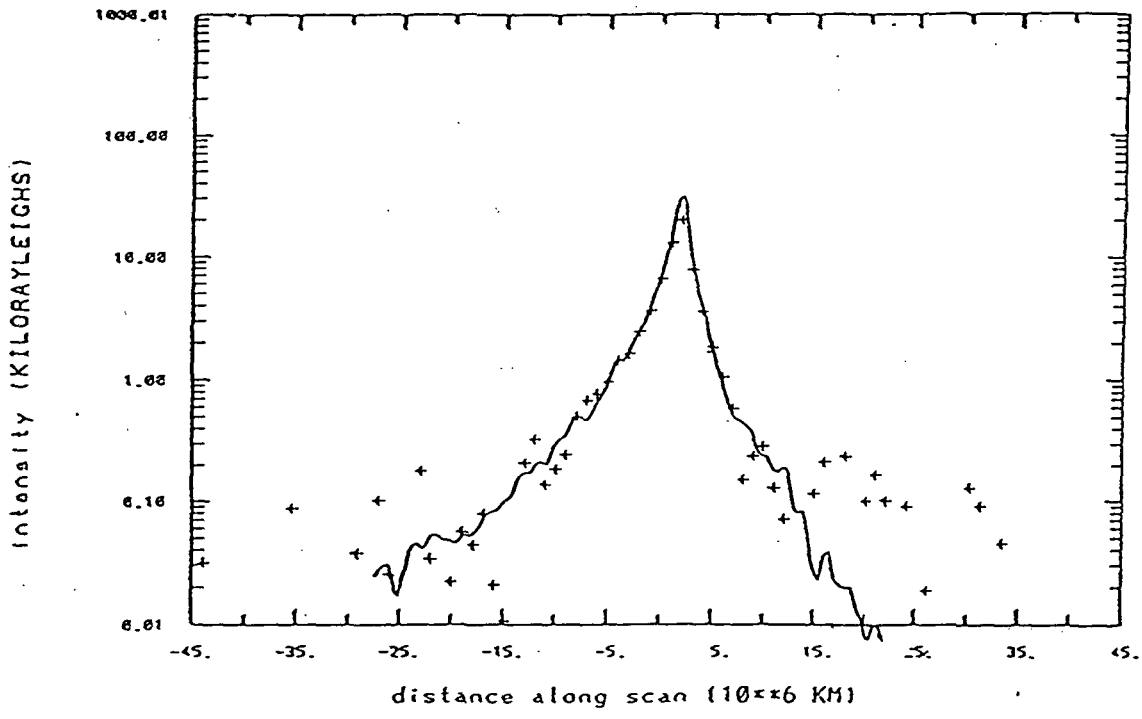
1000.01
100.00
10.00
1.00
0.10
0.01
Intensity (KILORAYLEIGHS)
-45.
-35.
-25.
-15.
-5.
5.
15.
25.
35.
45.
distance along scan (10**6 KM)

Figure 1

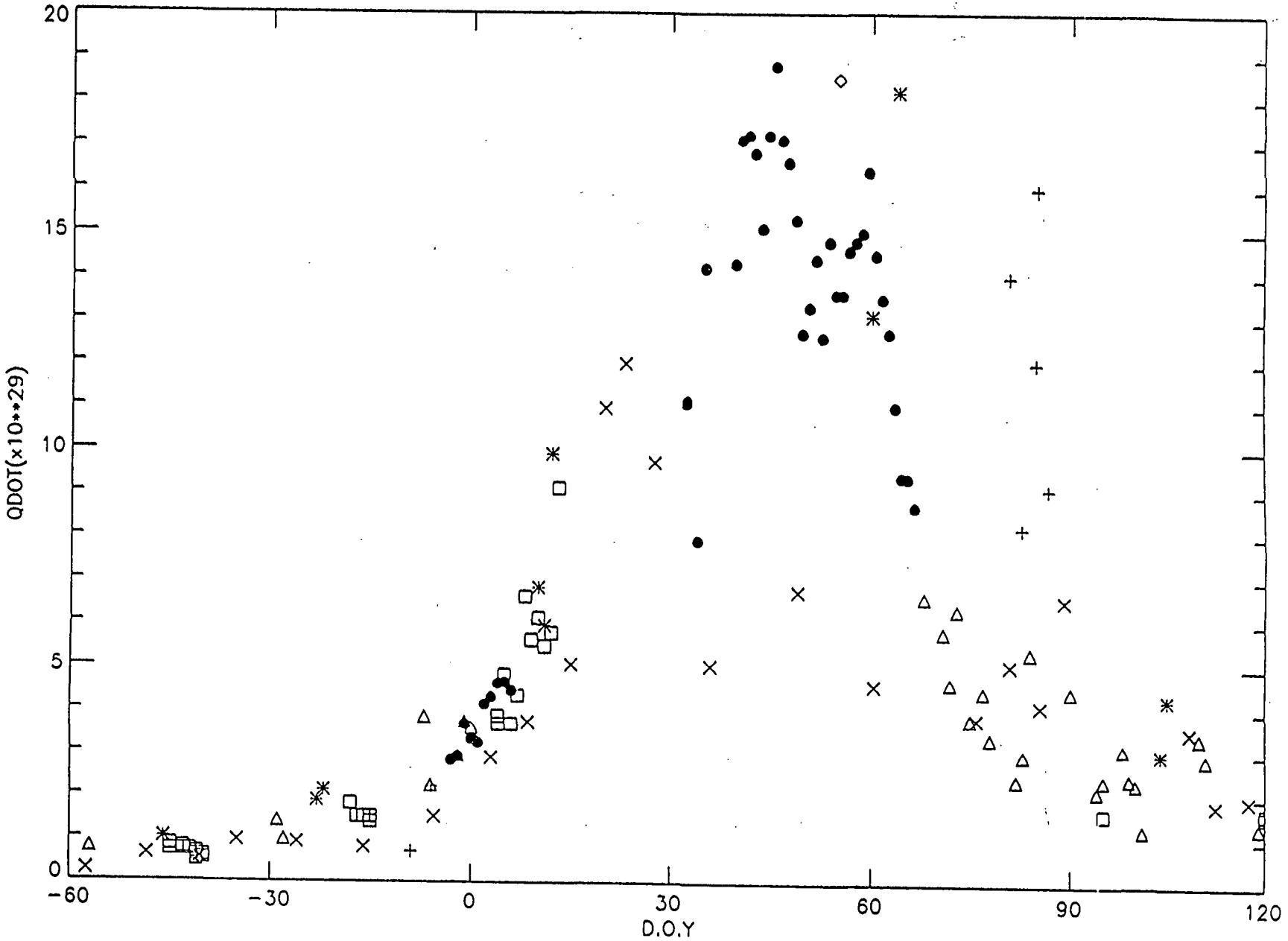

Figure 2

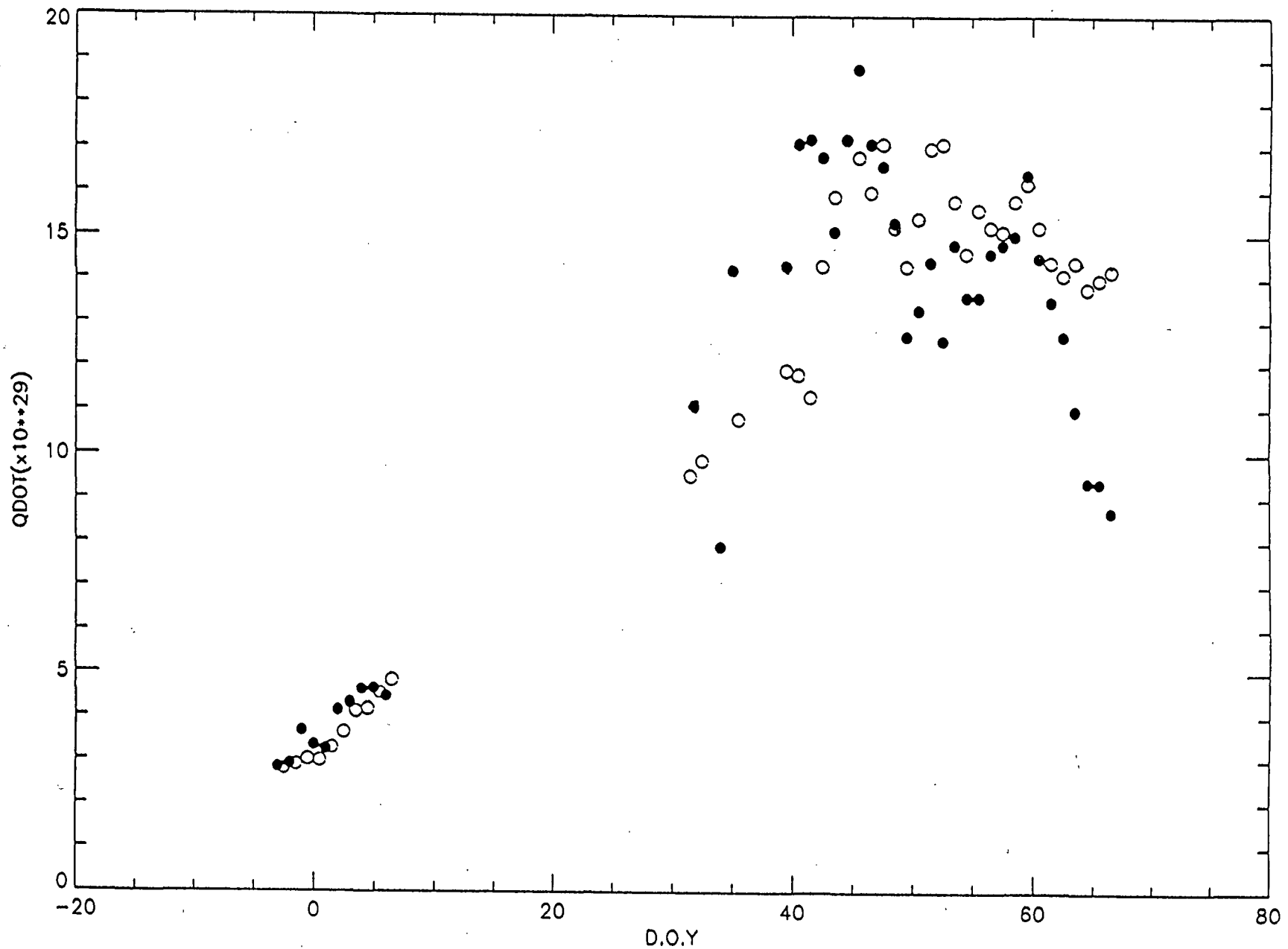

Figure 3

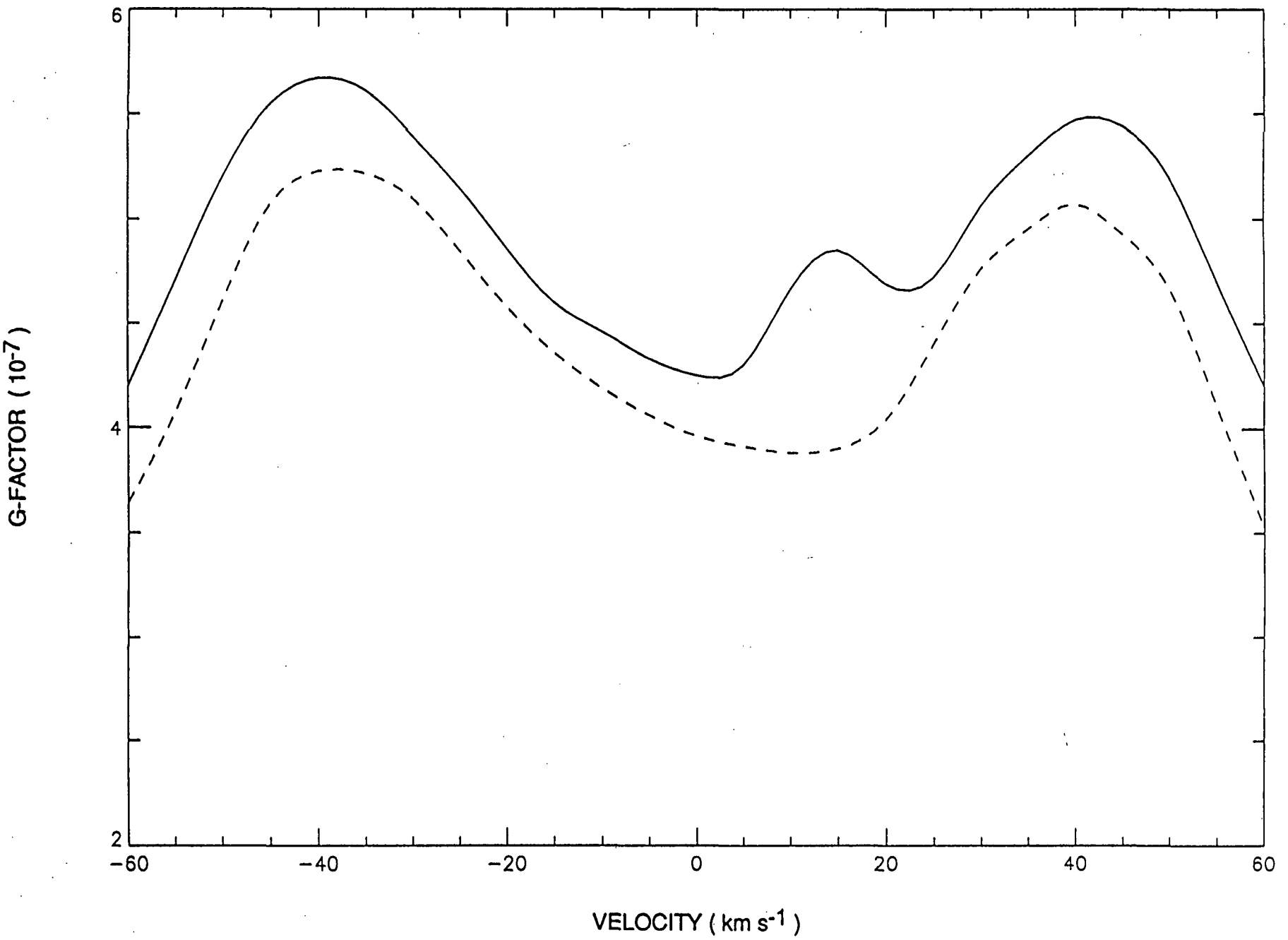

Figure 4

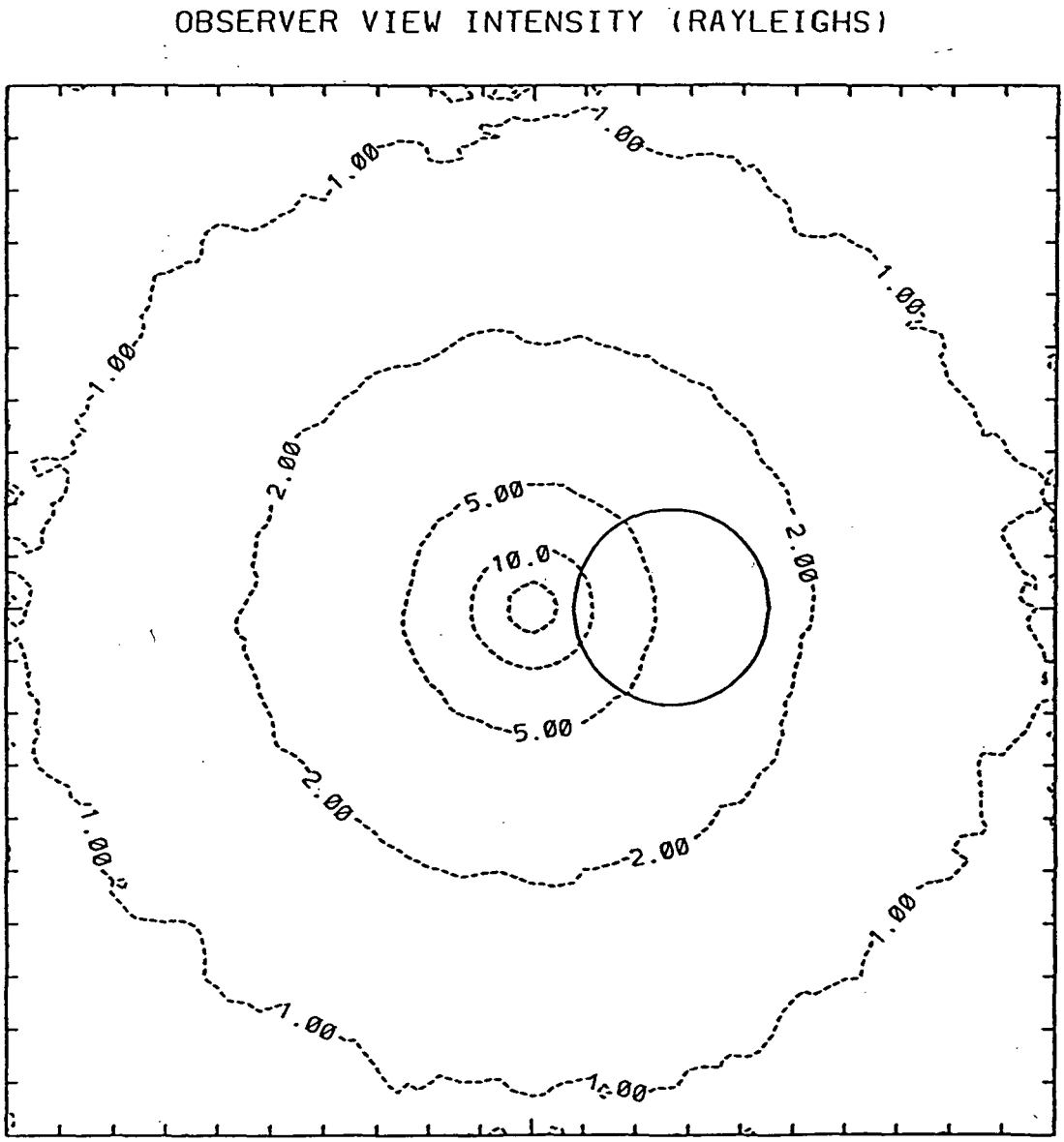
OBSERVER VIEW INTENSITY (RAYLEIGHS)
1.00
1.00
1.00
1.00
1.00
2.00
5.00
10.0
5.00
2.00
2.00
2.00
1.00
1.00
1.00
1.00
1.00
DISTANCE FROM THE NUCLEUS (BOX SIZE= 1.00E+05KM)

Figure 5

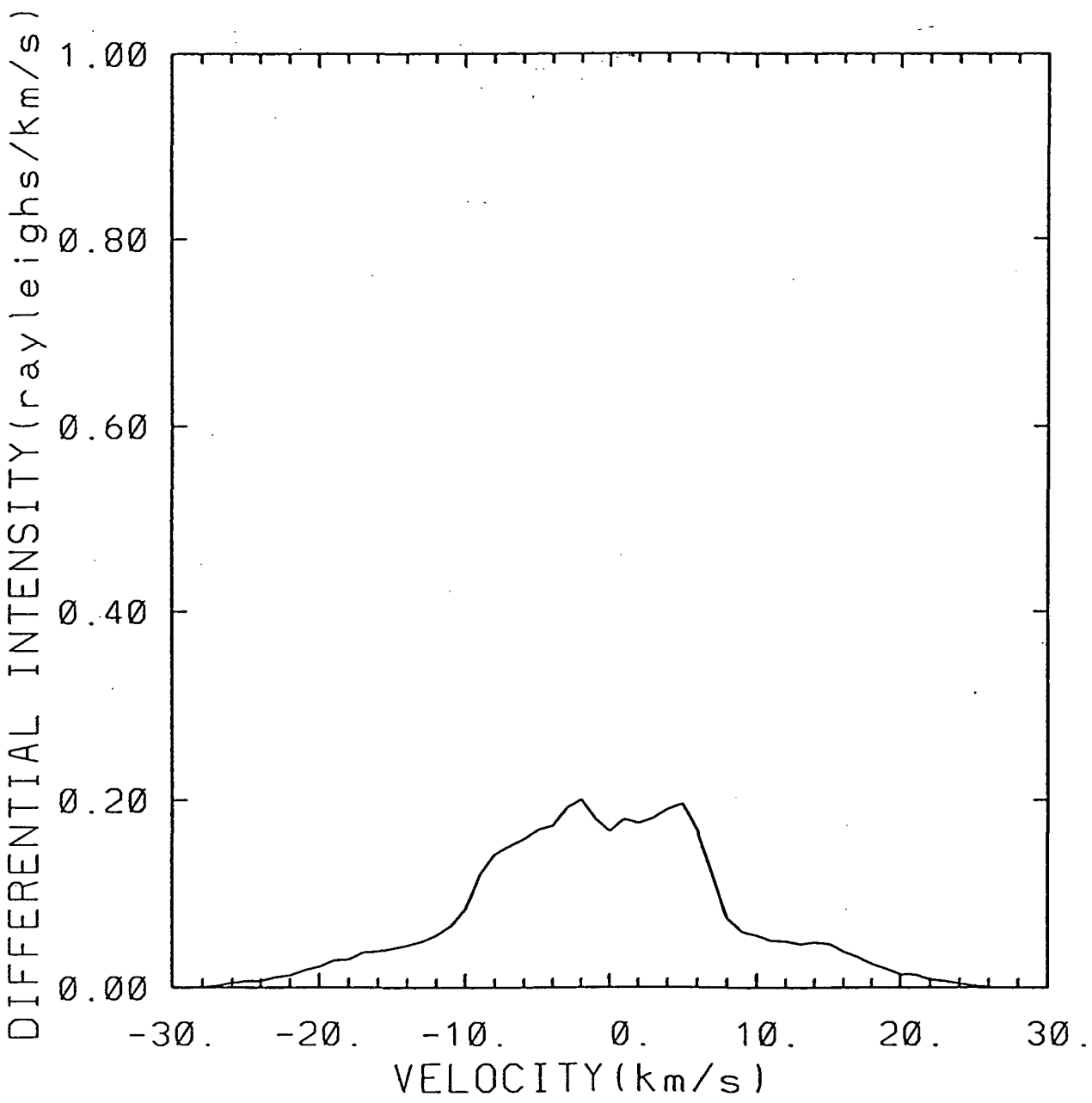
DIFFERENTIAL INTENSITY(rayleighs/km/s)
1.00
0.80
0.60
0.40
0.20
0.00
-30.
-20.
-10.
0.
10.
20.
30.
VELOCITY(km/s)

Figure 6

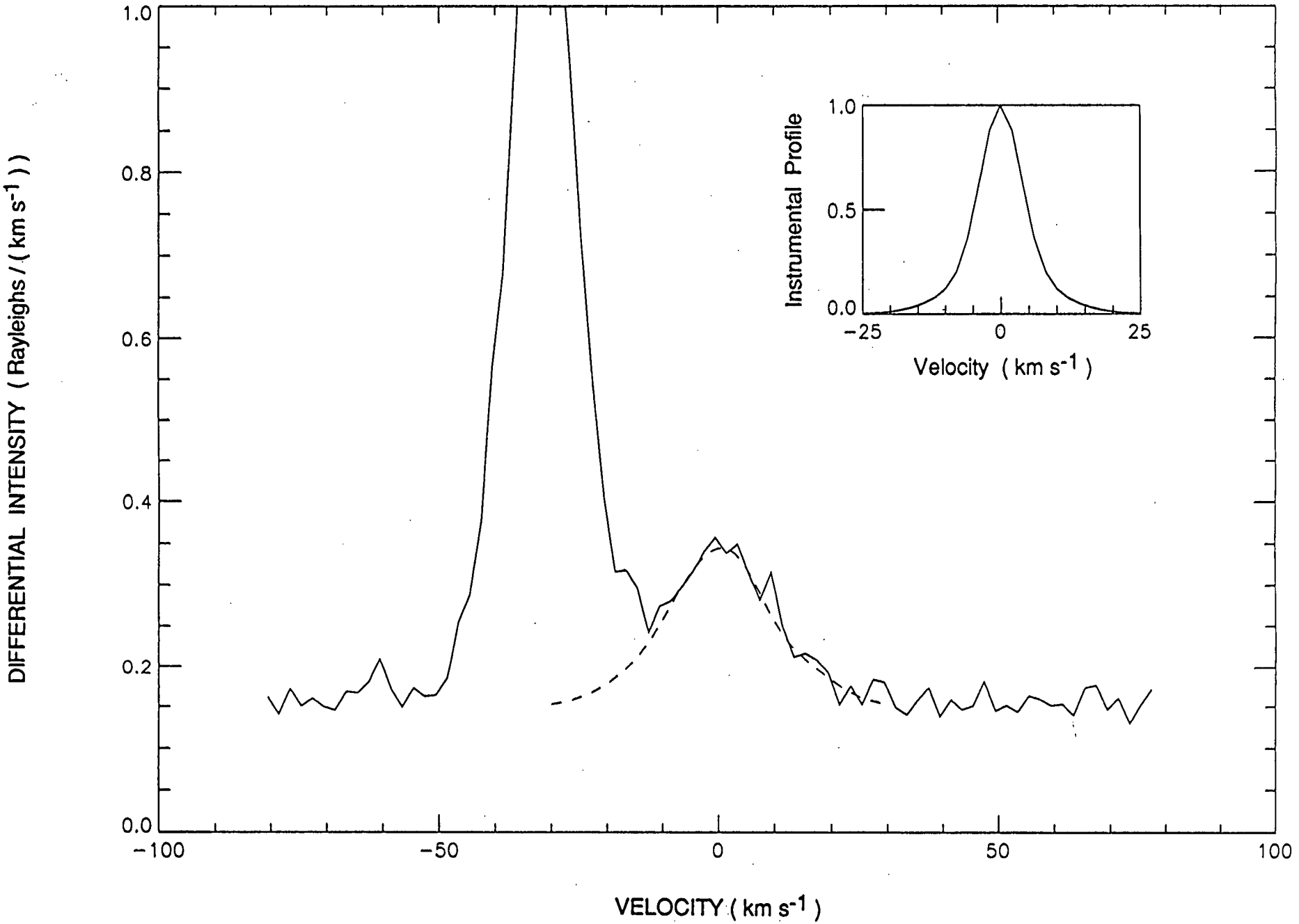
DIFFERENTIAL INTENSITY (Rayleighs / (km s-1))
1.0
0.8
0.6
0.4
0.2
0.0
−100
−50
0
50
100
VELOCITY (km s-1)
Instrumental Profile
1.0
0.5
0.0
−25
0
25
Velocity (km s-1)

Figure 7

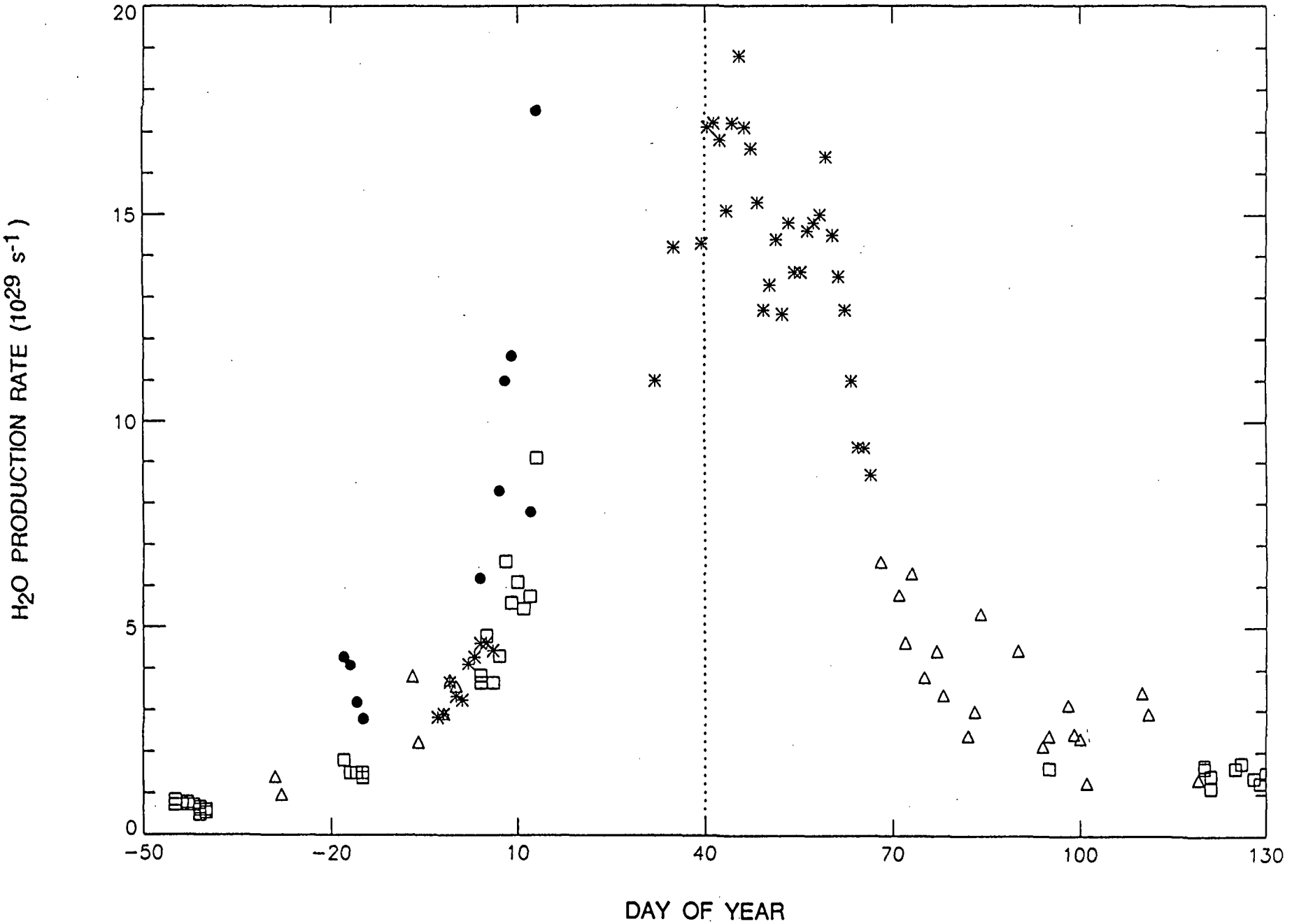
20
15
10
5
0
−50
−20
10
40
70
100
130
H2O PRODUCTION RATE (10^29 s^-1)
DAY OF YEAR

Figure 8

Appendix A

Analyses of the Pioneer-Venus Lyman-α Image of the Hydrogen Coma of Comet P/Halley

American Association for the Advancement of Science

SCIENCE

30 August 1991 $6.00
Vol. 253 ■ Pages 941–1064

Analysis of the Pioneer-Venus Lyman-α Image of the Hydrogen Coma of Comet P/Halley

WILLIAM H. SMYTH,* MICHAEL R. COMBI, A. I. F. STEWART

Comet Halley passed within 0.27 astronomical unit of Venus on 4 February 1986, 5 days before perihelion. This provided a unique opportunity to observe the comet's coma with the ultraviolet spectrometer orbiting the planet aboard the Pioneer Venus Orbiter spacecraft when the coma was otherwise obscured from Earth's view by the sun's glare. More than 9000 data points acquired systematically over the 5-day period from 2 to 6 February were combined to construct an excellent Lyman-α image of the hydrogen coma. The Lyman-α image was successfully reproduced with a comprehensive physical model, thereby verifying and documenting the underlying chemical kinetics and dynamics of the hydrogen coma.

WATER MOLECULES, THE DOMINANT volatile constituent sublimated from the surfaces of comets by solar heating, undergo multistep photodissociative reactions that liberate fast H atoms (*1–3*). For an active comet such as Halley, a collision-dominated zone develops around the nucleus. Within this zone, the fast atoms are thermalized or partly thermalized before escaping into the outer collision-free region where they form an enormous H coma, tens of millions of kilometers across. The shape of this coma depends on the interplay between the velocity distribution of the atoms, solar gravity, the antisolar acceleration produced by radiation pressure on the atoms, and (at large distance) the lifetime of the H atoms in the solar-wind environment. A satisfactory explanation of the detailed shape of the H coma of comet Kohoutek (*4*) was not achieved until a model incorporating a physical, unparameterized description of the collision zone was developed (*5–7*). Halley's H coma, which was imaged three times in 1216 Å ultraviolet (Lyman-α) light during its 1986 apparition, provides a second comet with a higher gas production rate and a much larger perihelion distance to test the physical picture noted above. We have analyzed the first of these images, obtained from the Pioneer Venus Orbiter Ultraviolet Spectrometer (PVOUVS) (*8*) a few days before perihelion, and have verified that the detailed physics and photochemistry incorporated in the model provide an excellent match to the image. The PVOUVS image was obtained during a period when the comet's conjunction with the sun rendered measurements from Earth extremely difficult. The other two images were obtained from sounding rockets some weeks after perihelion (*9*).

Observations of solar resonance–excited species in the comae of comet P/Halley by PVOUVS were obtained daily from 28 December 1985 through 7 March 1986, except for the period 7 to 30 January 1986 when Venus's superior conjunction interrupted the downlink to Earth. A description of the spacecraft and observing procedures and a presentation of the one-dimensional intensity scan data for the H, O, and C comae were reported by Stewart (*10*). The observing geometry over the 5-day period from 2 to 6 February, which provided this excellent out-of-the-plane Lyman-α image of the asymmetric hydrogen coma for PVOUVS but not for Earth, is illustrated in Fig. 1. Also shown in Fig. 1 is a simplified diagram of the spin-stabilized Pioneer Venus Orbiter showing that the optical axis of the ultraviolet spectrometer is fixed at about 60° from the spin axis and hence traces out a cone in the sky plane with each rotation of the spacecraft (approximately once every 13.5 s). The spacecraft spin axis, and hence the spectrometer field-of-view scan line across the sky, was held fixed for the 5-day imaging period. The comet's motion in the sky then carried its coma across this scan line, thereby mapping a two-dimensional region about the comet. Each scan line is composed of up to 128 samples along the portion of the complete cone sampling the coma and corresponds to a swath 1.4° wide through the coma. Typically 50 to 100 separate scan lines were added to improve the signal-to-noise ratio of each sample (or data point) along the scan.

Three possible sources contribute to the measured Lyman-α intensity at each data point: the comet, the Venus H corona, and the interplanetary background. The contribution from the Venus corona is negligible because observations of the comet were not made when the orbiter was near periapsis. The spatially dependent interplanetary background originates from the resonance scattering of solar Lyman-α photons by interstellar H atoms streaming through the solar system. The background contribution to each of the data points, which we determined using the interstellar hydrogen model of Ajello (*11*), was subtracted. We then constructed the cometary Lyman-α intensity image by spatially sorting the corrected data points (*12*). The resulting contour plot of the image is shown in Fig. 2. Superimposed over the contour map are dots marking the location of the over 9000 data points.

We analyzed the Lyman-α image using an updated version (*7*) of the fully time-dependent three-dimensional Monte Carlo particle trajectory model (MCPTM) of Combi and Smyth (*5, 6*). This model has

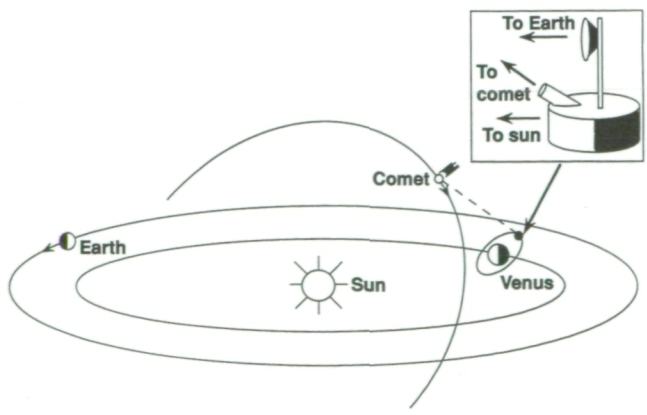

Fig. 1. Observing geometry of the Pioneer Venus Orbiter for comet P/Halley near perihelion. The relative positions to the sun of Earth, Venus, the comet, and the spacecraft on their orbits are shown. On 4 February 1986, the observational midpoint of the Lyman-α image data, the phase angle of the comet was 108°. The close-up of the Orbiter illustrates its spin-stabilized platform on which the ultraviolet spectrometer is located.

W. H. Smyth, Atmospheric and Environmental Research, Inc., Cambridge, MA 02139.
M. R. Combi, Space Physics Research Laboratory, University of Michigan, Ann Arbor, MI 48109.
A. I. F. Stewart, Laboratory for Atmospheric and Space Physics and Department of Astrophysical, Planetary, and Atmospheric Science, University of Colorado, Boulder, CO 80309.

*To whom correspondence should be addressed.

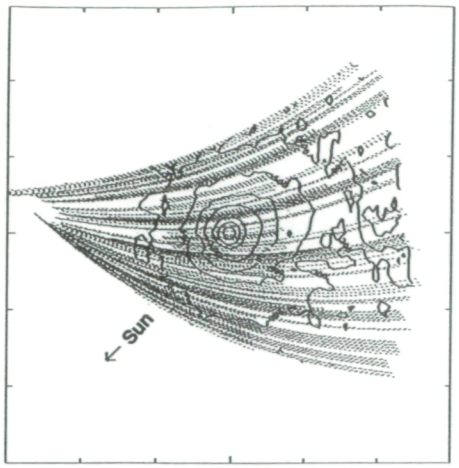

Fig. 2. Pioneer Venus Orbiter ultraviolet spectrometer image of comet Halley. A contour plot of the hydrogen Lyman-α emission from comet Halley, as seen by the PVOUVS during the period 2 to 6 February 1986, is shown with the contour levels in kilorayleighs of 0.2, 0.5, 1, 2, 5, 10, and 20. The tick marks on the circumscribed box are separated by 10×10^6 km. The map was constructed from over 9000 spin-scan data points, the locations of which are denoted by dots.

already been used successfully for analyzing PVOUVS observations of comets P/Giacobini-Zinner (*13*) and the published rocket observations (*4*) of comet Kohoutek (*6*). Whereas other earlier models used a parameterized atom velocity distribution to reproduce the shape of the H coma (*4*), this model predicts this distribution (and hence the coma shape) through its explicit description of the photolysis of water and the collision zone. Our treatment also allows for the effects of multiple scattering of Lyman-α photons in the inner coma, by means of a plane-parallel radiative transfer calculation (*14*). The Lyman-α flux for the sun in the model was taken from observations by the Solar Mesosphere Explorer corrected for solar rotation to the comet's heliocentric longitude. The time-dependent and spherically symmetric inner coma description used for the model was taken from a set of coupled dusty gas–dynamic and MCPTM calculations (*7*), which self-consistently explained most aspects of the heliocentric distance dependence of the outflow speed of the coma as inferred from widely varied sets of observations of the comet. In this inner coma description, the water production rate has been assumed to be 80% of the total gas production rate to account for species other than water (*15*).

In the H coma MCPTM, the remaining adjustable parameter is the H lifetime. This lifetime in the interplanetary environment is determined by three processes: charge exchange with solar-wind protons (by far the most important), photoionization by solar ultraviolet photons, and electron impact ionization by solar-wind electrons (*13*). There was no continuous monitoring of the solar-wind conditions in the space surrounding comet Halley except for the brief time before and after the spacecraft flybys. To compensate for this factor, we have collected much of the solar-wind data taken by the ISEE-3 (International Sun-Earth Explorer) and IMP-8 (Interplanetary Monitoring Platform) satellites (*16*) during this period and find an average lifetime for H atoms during the month of January of 2×10^6 s at 1 astronomical unit (AU).

The first model calculation of the two-dimensional Lyman-α image in Fig. 2 reproduced the innermost coma very well, but in portions of the outer coma below about 0.2 kR the modeled intensity fell below the observed level. This could be caused by (i) an underestimation of the H lifetime in the model, (ii) a radical increase in select portions of the actual time-dependent gas production rate not included in the model, or (iii) an underestimation of the Lyman-α background correction in the data.

Increasing the H lifetime even to an unrealistically large value of 3×10^6 s or more (reduced to 1 AU) increased the amount of H in the model at large distances from the nucleus and improved the fit to the image out to the 0.1- to 0.2-kR level. Beyond this distance, however, in the model the Lyman-α intensity again fell below the observed brightness. Of course, increasing the gas production rate during the period about 2 to 4 weeks before 4 February could reproduce the image at large cometocentric distances. However, the type of time variability required was severely at odds with the significant amount of excellent data used to determine the dependence of the gas production rate on the heliocentric distance (*7*). The effects of short-term variations in the water production rate are readily seen in the inner coma (*10*), but at the greater distances involved here they are strongly averaged by the wide dispersion of "ages" of atoms observed along a given line of sight. Only long-term changes are relevant.

A detailed examination of the radial profile of the image data in Fig. 2 (already corrected for the assumed interplanetary background), however, revealed that the inferred comet signal became independent of distance from the nucleus at large distances, a nonphysical result. This indicated that the background brightness initially assumed had to be larger by about 0.069 kR (that is, about 20%). With this larger interplanetary background, the new comet image can be well understood, even down to the 0.05-kR level. Furthermore, the image now makes physical sense (independent of the model) and agrees with the model using the H lifetime of 2×10^6 s at 1 AU. The corrected Lyman-α image and its comparison with the MCPTM calculation are shown in Fig. 3.

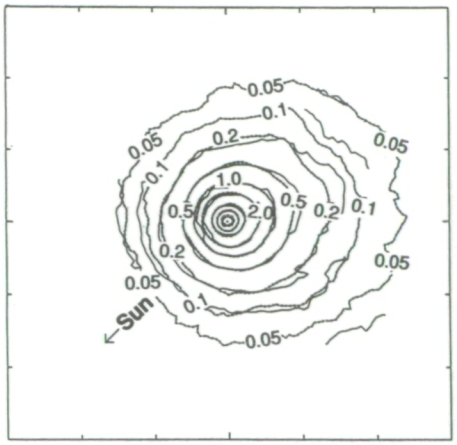

Fig. 3. The MCPTM analysis of the PVOUVS Lyman-α image. The isophote contours from PVOUVS observation (solid line), where an additional uniform background of 0.0692 kR has been subtracted, are compared with the best MCPTM result (dashed lines) which implies values of 2×10^6 s for the H lifetime (reduced to 1 AU) and 1.55×10^{30} s^{-1} for the water production rate during the period 2 to 6 February when the data were taken. The tick marks on the circumscribed box are separated by 10×10^6 km. Comparable models for the beginning and end of the 5-day period showed that the projected view of the comet did not change significantly and that the midpoint-time model was appropriate. The comet was essentially viewed from directly below its orbit plane, and the main temporal change, which was the rotation of the comet-sun line in the sky, had already been removed by the map sorting procedure.

The larger Lyman-α background in the comet image raises some interesting questions for other PVOUVS measurements, which are also directed toward improving the interstellar H model of Ajello (*11*) used here as an initial background correction. This model derived a best fit to a data set acquired over a period of 10 weeks, assuming that the interstellar H was uniformly illuminated by solar Lyman-α radiation throughout. One idea that is being pursued to understand this 20% increase is that the solar output at the Lyman-α wavelength has a longitudinal variability large enough so that the interstellar H and cometary H, which are at different heliocentric longitudes, may actually be subject to significantly different intensities for solar resonance scattering. Further work is required to evaluate the merit of this and other ideas.

The best fit of the model to the PVOUVS image in Fig. 3 implies a water production rate of 1.55×10^{30} s^{-1} during the midpoint of the observation. This production rate is ~30% higher than that published in the first

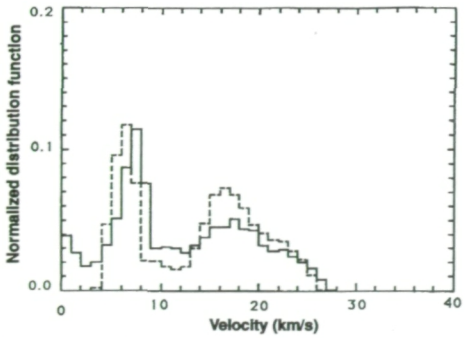

Fig. 4. Velocity distribution function for H atoms leaving the inner coma of comet Halley. The dashed line shows the distribution of velocities of H atoms as initially produced by photodissociation. The solid line shows the actual distribution function for atoms leaving the inner coma after partial collisional thermalization. Thermalization reduces the 20 km/s region and populates the region of low speeds (0 to 4 km/s), which initially contains no atoms.

analysis of these data (*10*), which was based only on the inner region of the coma and did not take into account the optical thickness of the inner coma to solar Lyman-α radiation. The MCPTM analysis of the entire extended image shows that the model (corrected for the optical thickness that occurs only in the inner coma) self-consistently reproduces the two-dimensional shape and gradient of the whole observable inner and outer coma. This result implies that the entire PVOUVS Lyman-α data set should be reevaluated, because all of the production rates determined from the Lyman-α data are likely to be systematically too low, at least where the derived production rates are large. The agreement of the model and data in Fig. 3 is most gratifying in that it both verifies and documents the advantage and value of using the physical model. Together with the analysis of comet Kohoutek (*6*), this analysis represents the second major and successful application of the full H MCPTM for a comet for which the gas production rate is sufficiently large that significant collisional thermalization occurs in the inner coma. Figure 4 shows the distribution in phase space of the velocities of H atoms leaving the inner coma as they are initially produced by photodissociation and after they are partially collisionally thermalized. The MCPTM naturally produces the correct number of low-speed H atoms that are required to explain the shape of the coma. This obviates the need for using a parameterized velocity distribution in the model (*4*).

REFERENCES AND NOTES

1. M. C. Festou, *Astron. Astrophys.* **96**, 52 (1981).
2. D. G. Schleicher, thesis, University of Maryland (1983).
3. E. F. van Dishoeck and A. Dalgarno, *Icarus* **59**, 305 (1984). The initial ejection speed distribution for H has been modified according to the new water solar photodissocation results of J. Crovisier, *Astron. Astrophys.* **213**, 459 (1989).
4. R. R. Meier *et al.*, *Astron. Astrophys.* **52**, 283 (1976).
5. M. R. Combi and W. H. Smyth, *Astrophys. J.* **327**, 1026 (1988).
6. ———, *ibid.*, p. 1044.
7. M. R. Combi, *Icarus* **81**, 41 (1989).
8. A. I. F. Stewart, *IEEE Trans. Geosci. Remote Sensing* **GE-18**, 65 (1980).
9. R. P. McCoy, C. B. Opal, G. R. Carruthers, *Nature* **324**, 439 (1986). The other two Lyman-α images were acquired by rocket payload instruments on 24 February and 13 March 1986.
10. A. I. F. Stewart, *Astron. Astrophys.* **187**, 369 (1987).
11. J. M. Ajello, *J. Geophys. Res.* **95**, 14855 (1990).
12. The data points were mapped into a polar coordinate system in which the polar angle was measured from the plane containing the comet, the sun, and the Pioneer Venus spacecraft. The radial coordinate was the perpendicular distance from Halley's nucleus to the instantaneous line of sight of the ultraviolet spectrometer. A grid of square sort boxes was laid out on the mapping plane; data points falling within the same box were averaged together, and empty boxes were filled by interpolation.
13. M. R. Combi, A. I. F. Stewart, W. H. Smyth, *Geophys. Res. Lett.* **13**, 385 (1986).
14. M. B. McElroy and Y.-L. Yung, *Astrophys. J.* **196**, 227 (1975).
15. M. C. Festou *et al.*, *Nature* **321**, 361 (1986).
16. R. Zwickl, personal communication.

17. The PVOUVS data used here were obtained and reduced under National Aeronautics and Space Administration (NASA) contract NAS2-12318. The modeling analysis and interpretation of the data were supported by the Planetary Atmospheres program of NASA under contracts NASW-3949 and NASW-3387. An earlier version of the Lyman-α image was released to the press in 1986. It was prepared by A. Jain of the University of California at Davis using data supplied by one of us (A.I.F.S.).

14 March 1991; accepted 25 June 1991

COVER This image of the enormous hydrogen coma surrounding Comet Halley was obtained by the Pioneer Venus Orbiter over a 5-day period in early February 1986. The image was constructed from over 9000 data points that were obtained as the spin axis of the rotating spacecraft was held fixed and the comet drifted across the instrument field of view. The false-color image, embellished by white constant-brightness contours, shows the Lyman-α brightness distribution at 1216 angstroms. The spacecraft is now headed toward a fiery death in the upper atmosphere of Venus in the fall of 1992. See page 1008. [Image processing by A. I. F. Stewart and M. R. Combi]

Appendix B

Planetary Equations for the Outer Planet-Satellite Systems

Appendix B. Planetary Equations for the Outer Planet-Satellite Systems

For an H atom, the planetary oblateness and the solar radiation pressure acceleration provide small perturbations to the normal force experienced from the spherically symmetric r^{-1} gravitational potential of the planet. This means that the orbital elements of the H atoms that describe its orbit about the planet change slowly from their initial values. The orbital trajectory of an atom may be solved straightforwardly by solving Newton's equations of motion for these three forces. However, another approach, which is more computationally efficient, is to solve the planetary equations for the slowly varying orbital elements where the two perturbing forces are only included to first order. This latter approach is discussed below.

The classical description of the location of an object on its orbit in three dimensions is specified by the six orbital elements of the object and their time dependence (see, for example, Roy 1965). The six orbital elements for perturbed Keplerian motion for planetary bound orbits are

a = semimajor axis (in units of the planetary radii R)

e = eccentricity

i = inclination of the orbital plane to the equator plane

Ω = right ascension of the ascending node

ω = argument of perigee

M = mean anomaly = n (t - T)

where t is the time, T is the time of periapsis passage and n is the mean angular velocity given by

$$n^2 = \frac{\mu}{a^3 R^3}$$

where $\mu = GM_N$ is the product of the gravitational constant times the mass of the planet. The planetary equations for the period–averaged orbital elements $\left(\bar{a},\bar{e},\bar{i},\bar{\Omega},\bar{\omega},\bar{M}\right)$, which determined their long-time evolution, when the two perturbation forces have been included to first order, have been derived and are given as follows:

$$\frac{d\bar{a}}{dt} = 0 \tag{1}$$

$$\frac{d\bar{e}}{dt} = \frac{3}{2}\frac{\left(1-\bar{e}^2\right)^{1/2}}{\tau_0}\left[\left(\cos\bar{\Omega}\sin\bar{\omega}+\sin\bar{\Omega}\cos\bar{\omega}\cos\bar{i}\right)\sin\phi+\sin\bar{i}\cos\bar{\omega}\cos\phi\right] \tag{2}$$

$$\frac{d\bar{i}}{dt} = \frac{3}{2\tau_0}\frac{\bar{e}}{\left(1-\bar{e}^2\right)^{1/2}}\cos\bar{\omega}\left(\sin\bar{\Omega}\sin\bar{i}\sin\phi-\cos\bar{i}\cos\phi\right) \tag{3}$$

$$\frac{d\bar{\Omega}}{dt} = \frac{\cos\gamma}{\left(\cos^2\gamma+\sin^2\gamma\sin^2\phi\right)}\lambda$$

$$+\frac{3}{2\tau_0}\frac{\bar{e}}{\left(1-\bar{e}^2\right)^{1/2}}\frac{\sin\bar{\omega}}{\sin\bar{i}}\left(\sin\bar{\Omega}\sin\bar{i}\sin\phi-\cos\phi\cos\bar{i}\right)-\frac{3}{2}\sqrt{\frac{\mu}{\bar{a}^3R^3}}\frac{J_2\cos\bar{i}}{\bar{a}^2\left(1-\bar{e}^2\right)^2} \tag{4}$$

$$\frac{d\bar{\omega}}{dt} = \frac{3}{2\tau_0}\frac{(1-\bar{e}^2)^{1/2}}{\bar{e}}\left[\left(\cos\bar{\Omega}\cos\bar{\omega}-\frac{\sin\bar{\Omega}\sin\bar{\omega}\cos\bar{i}}{1-\bar{e}^2}\right)\sin\phi\right.$$

$$\left.-\left(\sin\bar{i}\sin\bar{\omega}-\frac{\bar{e}^2}{1-\bar{e}^2}\frac{\sin\bar{\omega}\cos^2\bar{i}}{\sin\bar{i}}\right)\cos\phi\right]-\frac{3}{2}\sqrt{\frac{\mu}{\bar{a}^3R^3}}\frac{J_2}{\bar{a}^2\left(1-\bar{e}^2\right)^2}\left(\frac{5}{2}\sin^2\bar{i}-2\right) \tag{5}$$

$$\frac{d\bar{M}}{dt} = \sqrt{\frac{\mu}{\bar{a}^3 R^3}}\left\{ 1 - \frac{3}{2}\frac{f}{\left(\frac{\mu}{\bar{a}^2 R^2}\right)}\left(\frac{1+\bar{e}^2}{\bar{e}}\right)\left[\left(\cos\bar{\omega}\cos\bar{\Omega} - \cos\bar{i}\sin\bar{\omega}\sin\bar{\Omega}\right)\sin\phi\right.\right.$$

$$\left.\left. + \sin\bar{i}\sin\bar{\omega}\cos\phi\ \right] + \frac{3}{2}\frac{J_2}{\bar{a}^2}\frac{\left(1-\frac{3}{2}\sin^2\bar{i}\right)}{\left(1-\bar{e}^2\right)^{3/2}}\right\}. \qquad (6)$$

In addition we have that

$$\tau_0 = \frac{1}{f}\sqrt{\frac{\mu}{\bar{a}R}}$$

and

$$\cos\phi = -\sin\gamma\cos(\lambda t + \alpha_0).$$

In the above equations, λ is the mean angular motion of the planet around the sun, f is the solar radiation pressure acceleration experienced by H atoms at the planet, J_2 is the standard gravitational oblateness parameter for the planet, γ is the obliguity of the planet and α_0 is an angle which allows the initial position of the sun to be specified in the sky plane of the planet.